CHROMATIN FIBERS ARE LEFT-HANDED DOUBLE HELICES WITH DIAMETER AND MASS PER UNIT LENGTH THAT DEPEND ON LINKER LENGTH

SHAWN P. WILLIAMS, BRIAN D. ATHEY, LOUIS J. MUGLIA, R. SCOTT SCHAPPE, ALBERT H. GOUGH, AND JOHN P. LANGMORE

Biophysics Research Division and Division of Biological Sciences, University of Michigan, Ann Arbor, Michigan 48109

ABSTRACT Four classes of models have been proposed for the internal structure of eukaryotic chromosome fibers—the solenoid, twisted-ribbon, crossed-linker, and superbead models. We have collected electron image and x-ray scattering data from nuclei, and isolated chromatin fibers of seven different tissues to distinguish between these models. The fiber diameters are related to the linker lengths by the equation: $D(N) = 19.3 + 0.23\ N$, where $D(N)$ is the external diameter (nm) and N is the linker length (base pairs). The number of nucleosomes per unit length of the fibers is also related to linker length. Detailed studies were done on the highly regular chromatin from erythrocytes of *Necturus* (mud puppy) and sperm of *Thyone* (sea cucumber). *Necturus* chromatin fibers ($N = 48$ bp) have diameters of 31 nm and have 7.5 ± 1 nucleosomes per 10 nm along the axis. *Thyone* chromatin fibers ($N = 87$ bp) have diameters of 39 nm and have 12 ± 2 nucleosomes per 10 nm along the axis. Fourier transforms of electron micrographs of *Necturus* fibers showed left-handed helical symmetry with a pitch of 25.8 ± 0.8 nm and pitch angle of 32 ± 3°, consistent with a double helix. Comparable conclusions were drawn from the *Thyone* data. The data do not support the solenoid, twisted-ribbon, or supranucleosomal particle models. The data do support two crossed-linker models having left-handed double-helical symmetry and conserved nucleosome interactions.

INTRODUCTION

Chromatin fibers are composed of a repeating subunit called the nucleosome (reviewed by McGhee and Felsenfeld, 1980; Igo-Kemenes et al., 1982). The nucleosome consists of a highly conserved "core" containing 146 bp of DNA associated with a globular histone octamer, and a tissue-specific "linker" containing 20–100 bp of DNA associated with the tissue-specific histone, H1. The core is a flat disk ~5.7 nm high and 11 nm in diameter with 1¾ left-handed turns of DNA wrapped around the short axis of the histone octamer (Richmond et al., 1984). The physiologically relevant structure of transcriptionally inactive genes in eukaryotic cells is the thick chromatin fiber, usually measured by electron microscopy to be 20–30 nm in diameter (e.g., Tomlin and Callan, 1951; Gall, 1963; Davies, 1968; Finch and Klug, 1976).

Models for the Structure of Chromatin Fibers

There are three classes of helical models for chromatin fibers: the solenoid, twisted-ribbon, and crossed-linker models. Additionally, there is a nonhelical class, called the supranucleosomal particle models. Each class of models has common features that distinguish its members from those of other classes. We maintain that none of these classes is excluded by the hydrodynamic, optical, microscopic, or diffraction measurements yet reported.

The solenoid class of models (Fig. 1 *a*, *b*) was proposed by Finch and Klug (1976), who were motivated by their observation of a 11 nm-wide column of nucleosomes (the nucleofilament) at low ionic strength. The solenoid was proposed to be 25–30 nm in diameter with 5–7 nucleosomes per turn. The linker DNA is wrapped in a helical path between the nucleosome cores, leaving a central hole (e.g., Notbohm et al., 1979; McGhee et al., 1983). Although the helical pitch is constrained by the width of the nucleosome, there are no inherent constraints upon fiber diameter, mass per unit length, or handedness of the helix. The distinguishing features of the solenoid are: (*a*) a sequential arrangement of nucleosomes along a single helical ramp; (*b*) a pitch of ~11 nm; (*c*) a solvent-filled space in the center; (*d*) nonconserved interactions among nucleosome cores, which depend on linker length; and (*e*) an asymmetric unit consisting of a variable number of nucleosomes, depending on linker length. Butler (1984) has proposed a modified solenoid model, with linker DNA kinked into the center to conserve fiber diameter, mass per unit length, and nucleosome interactions.

The twisted-ribbon class of models (Fig. 1 *c*, *d*) was proposed by Worcel et al. (1981) and Woodcock et al. (1984), who were motivated by observations of zigzag

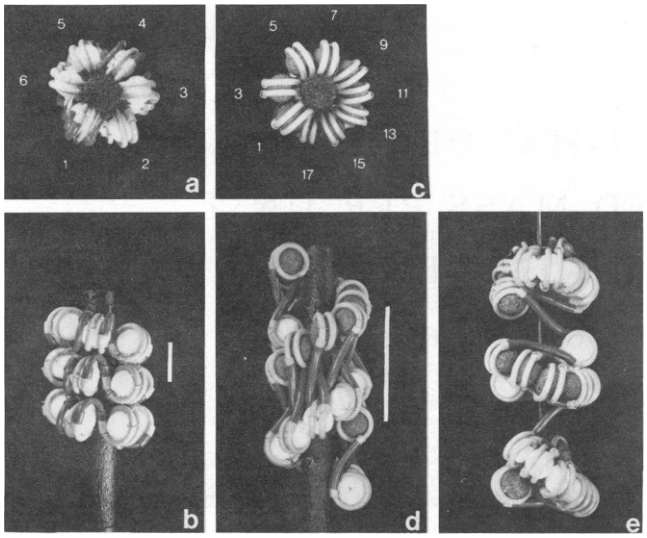

FIGURE 1 Space-filling models illustrating three major classes of structures proposed for chromatin. Core DNA is shown in gray; linker DNA (N = 48 bp, as in Necturus erythrocytes) is shown in red. Numbers indicate the sequence of nucleosomes; vertical bars indicate helical pitch. (*a,b*) End-on and side-on views of the solenoid model. The model has a helical repeat of 6 nucleosomes; pitch of 11 nm; diameter of 30 nm; and central hole of 8.5 nm diameter. (*c,d*) End-on and side-on views of the twisted-ribbon model, showing the single ribbon of dinucleosomes consisting of the even [white] and odd [blue] nucleosome cores. The model has a helical repeat of 18 nucleosomes; pitch of 32 nm; diameter of 30 nm; and central hole of 8.5 nm diameter. (*e*) The supranucleosomal particle model, as constructed from a dislocated double-helical crossed-linker model. Please refer to the color figure section at the back of this book.

arrangements of nucleosomes at low ionic strength. The basic unit of the structure is a flat ribbon consisting of two parallel stacks of nucleosomes connected by relaxed spacer DNA. The ribbon is wrapped on the surface of a cylinder to form a fiber with linker DNA that zigzags up and down the helical axis. Worcel proposed that three different ribbons could be constructed, each with a characteristic linking number increment (ΔL), which describes the change in the DNA linking number per nucleosome. Worcel favored a $\Delta L = -1$ twisted-ribbon, based on the experimentally determined linking number of SV40 minichromosomes (Keller, 1975). Woodcock favored the $\Delta L = -2$ structure, because the DNA appeared to be more relaxed. There are no apparent constraints on the handedness or the diameter of the helix formed, although Woodcock et al. maintained that the diameter should be independent of linker length. The distinguishing features of the twisted-ribbon models are: (*a*) an alternating sequence of nucleosomes in a two-column ribbon wrapped into a single-start helix; (*b*) a helical pitch of 22 nm or more, depending upon the length and orientation of the linker DNA; (*c*) conserved interactions among nucleosomes; and (*d*) an asymmetric unit composed of two nucleosomes.

The crossed-linker models are nonsequential arrangements of nucleosomes cores connected by transverse linker DNA. These models can be characterized by the number of helical ramps in each helical repeat, *n*. Staynov (1983) proposed two crossed-linker models that form single-start ($n = 1$) left-handed helices, based upon the tendency of nucleases to produce dinucleosomes rather than mononucleosomes. Makarov et al. (1985) proposed a triple helix, based on their flow dichroism measurements. We propose two nearly indistinguishable crossed-linker models that form two-start ($n = 2$) left-handed helices (Fig. 2). Our motive was to satisfy the structural parameters determined by our electron microscopy and x-ray studies of highly ordered chromatin. The double-helical crossed-linker models are distinguished by: (*a*) an alternating sequence of nucleosomes in two equivalent helical ramps; (*b*) a pitch of ~26 nm; (*c*) transverse linker DNA that crisscrosses between nucleosome cores; (*d*) fiber diameters that vary linearly with linker length; (*e*) conserved interactions among nucleosomes; and (*f*) an asymmetric unit composed of a mononucleosome.

The fourth class of models is the supranucleosomal particle (or superbead) model (Fig. 1 *e*), first proposed by Renz et al. (1977) to account for the beaded appearance of the fibers prepared at intermediate ionic strength. Many sedimentation and microscopic experiments have identified a tendency of the fibers to fragment into globular domains of variable size (e.g., Zentgraf and Franke, 1984). These domains would have variable point symmetry or no symmetry. The particulate structures are consistent with

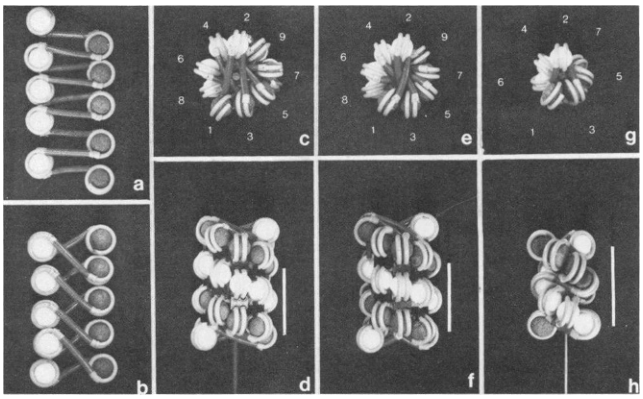

FIGURE 2 Space filling models illustrating the double-helical crossed-linker model. Core DNA is shown in gray; linker DNA in red; odd nucleosomes with blue cores; and even nucleosomes with white cores. Numbers indicate the sequence of nucleosomes; vertical bars indicate helical pitch. (*a–f*) Models with Necturus erythrocyte linker length (N = 48 bp). (*a,b*) Side-on views of extended ribbons of nucleosomes with $\Delta L = -1$ and -2. (*c,d*) End-on and side-on views of a double-helical crossed-linker model formed from a $\Delta L = -1$ ribbon. This model has a helical repeat of 18 nucleosomes; pitch (vertical bar) of 26 nm; diameter of 33 nm; and central hole of 3 nm diameter. (*e,f*) End-on and side-on views of a double-helical crossed-linker model formed from a $\Delta L = -2$ ribbon. This model has a helical repeat of 18 nucleosomes; pitch of 26 nm; diameter of 31 nm; and no central hole. (*g,h*) End-on and side-on views of a double-helical crossed-linker model formed from a $\Delta L = -1$ ribbon with short linker (N = 22 bp). This model has a helical repeat of 14 nucleosomes; pitch of 30 nm; diameter of 25 nm; and central hole of 3 nm diameter.

dislocations in the crossed-linker helical structures (as shown in Fig. 1 *e*), or in any of the other helical structures.

We will show that chromatin fibers are left-handed double helices with diameter and mass per unit length that depend on linker length. Our data are consistent with crossed-linker models having $n = 2$, shown in Fig. 2. Our data are not consistent with the solenoid, twisted-ribbon, or crossed-linker models having $n = 1$ or 3.

METHODS AND MATERIALS

Reagents

Buffer MB consisted of 60 mM KCl, 15 mM NaCl, 15 mM Pipes (pH 7.1), 3 mM $MgCl_2$, 0.02% NaN_3, and 0.1 mM phenylmethylsulfonyl fluoride (PMSF). Buffer EB was identical to MB, except 3 mM (ethylene dinitrilo) tetraacetic acid (EDTA) replaced the $MgCl_2$. MLB consisted of MB with 1 mM iodoacetate, and 0.3% Nonidet P-40 (NP-40) or 0.1% digitonin. WBH consisted of 130 mM NaCl, 5 mM KCl, 2 mM $MgCl_2$, and 10 mM Hepes (pH 7.0). SSW was prepared according to the instruction from a powder obtained from Instant Ocean (Eastlake, OH). Micrococcal nuclease from *Staphylococcus aureus* (EC 3.1.31.1) was stored frozen at 7,000 units/ml in MB. DNAse I (Sigma grade DN-EP, Sigma Chemical Co., St. Louis, MO) from bovine pancrease (EC 3.1.21.1) was stored frozen at 5 mg/ml in MB. Protease K was stored frozen at 0.1 mg/ml in water. Hae III restricted ΦX-174, and Hind III restricted lambda DNA (Bethesda Research Laboratories, Bethesda, MD) were used as DNA size markers. Concentrations of chromatin were measured by absorbance at 260 nm, assuming $A_{260} = 1$ for 50 μg/ml. All reagents were purchased from Sigma, unless otherwise noted. Rhode Island Red chickens were purchased from Dave's Poultry (Ann Arbor, MI); *Necturus maculosus* (mudpuppy) from Charles Sullivan (Nashville, TN) and North Carolina Biological Supply (Burlington, NC); *Strongylocentrotus purpuratus* (sea urchin) and *Pisaster giganticus* (sea star) from Alacrity Marine Biological Supply (Redondo Beach, CA); and *Thyone briarius* (sea cucumber) from Woods Hole Laboratory (Woods Hole, MA). Other materials were produced at the University of Michigan, including *Xenopus laevis* (gift of Mr. R. Gruschow), mouse G53 myeloma cells (gift of Dr. L. Claflin), CHO cells (gift of Dr. D. Oxender), and *Tetrahymena* cells (gift of Dr. S. L. Allen).

Nuclear Isolations

Erythrocytes, sperm, and tissue culture cells were collected and processed as described in Langmore and Paulson (1983), with the exception that 1 mM iodoacetate was included in the lysis buffers to inhibit the sulfhydryl proteases (Workman and Langmore, 1985). Erythrocytes were lysed first in MLB with digitonin, followed by three washes in MLB containing NP-40, a procedure that reduced aggregation. *Tetrahymena thermophilia* micronuclei were prepared according to Allen et al. (1983).

Determination of Nucleosome Repeat Length

Nuclei were suspended to 1 mg/ml in MB at 37°C. The suspension was made 1 mM in $CaCl_2$ and 200 units/ml micrococcal nuclease. The digestion was stopped after 0.5–6 min with 10 mM EDTA. The samples were digested for 4 h with 0.1 mg/ml Protease K, diluted to 0.25 mg/ml in sample buffer (25 mM Tris, pH 6.8, 0.5% sodium lauryl sulfate, 4% glycerol, 2% 2-mercaptoethanol, 0.0004% bromphenol blue), loaded as 5 μg aliquots onto 1.7% agarose gels made with 89 mM Tris, 89 mM boric acid, 2 mM EDTA, and electrophoresed for 4 h at 4 V/cm. Gels were stained with 0.5 μg/ml ethidium bromide, photographed by UV transillumination, and the negatives scanned with a Joyce Loebl Mk III microdensitometer (Gateshead-on-Tyne II, England). Fragment sizes were calculated from the mobility of the oligonucleosomes relative to the standards. The nucleosome repeat length was determined from the slope of a linear least-squares fit of the trimer through octamer molecular weights vs. oligomer number (Chambers et al., 1983).

Isolation of Chromatin

The reasons for studying *Necturus* erythrocyte chromatin were the large amount of inactive chromatin per cell, the high contrast in the diffraction patterns of nuclei, and the short nucleosome repeat length. *Necturus* nuclei were suspended to 1 mg/ml in MB containing 0.5 mM $CaCl_2$ rather than $MgCl_2$, and then digested with 20 units/ml of micrococcal nuclease for 8–10 min at ≈22°C. Digestion was stopped by adding 5 mM EDTA and chilling to 0°C, followed by centrifugation at 80 × *g* for 5 min. The pellet was resuspended to 1 mg/ml in 5 mM EDTA (pH 7.0) and incubated at 0°C for 10–20 min. Nuclear debris was removed by centrifugation for 30 min at 12,800 × *g*. Typically, 10–35% of the chromatin was solubilized. This procedure was used to minimize exposure of the chromatin to low ionic strength. We found it impossible to extract chromatin at the higher ionic strengths reported by Ruiz-Carrillo et al. (1980).

The reasons for studying *Thyone* sperm chromatin were the high contrast in the diffraction patterns, the long nucleosome repeat length, and that the chromatin appeared to be soluble as visualized by Tilney (1976) in thin sections. 1 mg/ml of *Thyone* nuclei in MB with 1.5 mM $CaCl_2$ were digested with 20 units/ml of micrococcal nuclease for 20–25 s at 37°C. Digestion was stopped with 10 mM EDTA and 0°C. After 10 min centrifugation at 12,800 × *g* ~25% of the chromatin remained in solution. Sea urchin and starfish sperm chromatin were not solubilized by this procedure, owing to the greater degree of chromatin compaction.

X-Ray Scattering

X-ray patterns were collected as described in Langmore and Paulson (1983) on a 138 cm Franks camera equipped with a position-sensitive detector (Technology for Energy Corporation, Knoxville, TN). To insure that the diffraction features arose exclusively from chromatin, control digestions of nuclei with DNAse I were performed according to Langmore and Paulson (1983); and also according to a high-salt protocol involving digestion of 1 mg/ml nuclei in MB with 0.2 mg/ml DNAse I for 1 h at 37°C, followed by two washes in an equal volume of 1 M NaCl, 2 mM $MgCl_2$, 10 mM Pipes, 0.2% azide, 0.1 mM PMSF. No proteolysis resulted from isolation or treatment of nuclei and chromatin, as assayed by SDS-PAGE according to the procedures of Langmore and Paulson (1983).

To be consistent with the microscopy, the text refers to the position of diffraction features in terms of the equivalent Bragg spacing (i.e., $1/s$, where $s = 2\sin(\theta/2)/\lambda$, with θ = scattering angle and λ = wavelength). Predicted diffraction from randomly oriented cylinders of infinite length was calculated from equations in Oster and Riley (1952), with the corrections of Porod (1948). The scattering for solid cylinders of different diameters was fit to the x-ray data in the range of $1/s = 18$–30 nm. The fit over the range $1/s = 18$–55 nm was further optimized by allowing solvent to fill the central 10–20% of the cylinders. To obtain the best fit for the width of the diffraction peak, the fibers diameter were given a gaussian distribution with 22% standard deviation. All fitting was done by eye, and was limited to low angles, because the cylindrical-object approximation is not valid for $1/s < 18$ nm, owing to structure within the fibers.

Electron Microscopy

Chromatin fibers were fixed in EB with 1.0% glutaraldehyde for ~24 h at 0°C, applied to freshly prepared carbon films, rinsed once with a few drops of water, and then negatively stained with 1–2% uranyl acetate or metal shadowed with Pt:Pd at an angle of 6° in a Denton model DV502 bell jar (Cherry Hill, NJ). The grids were inserted specimen-side-down into a JEOL JEM 100B electron microscope. The samples were examined

at 100 KeV at 44,000–66,000 × magnification. The magnification was calibrated at the end of each microscope session using a grating replica with 21,600 lines/cm (Ted Pella, Tustin, CA).

Fiber diameters were measured on fibers selected to be uniformly stained and straight. The fibers were positioned by eye on the Joyce Loebl densitometer and scanned perpendicular to the fiber axis with a slit size of 22 nm along the axis and 0.5 nm perpendicular to the axis. Fiber width was measured as the full width at half-maximum intensity of the densitometer tracing. The measured diameters were independent of electron microscope focus.

The electron images were digitized and analyzed with the Zeiss SEM IPS (Carl Zeiss, Thornwood, NY) with a 4-megabyte array processor. The micrographs were recorded using a dissection microscope (Bausch and Lomb, Rochester, NY) with a newvicon camera (Model 60, Dage MTI, Michigan City, IN). 512 × 512 pixel images were recorded, "masked and floated," Fourier-transformed, and the transform intensities recorded on film in <5 min. The system was calibrated using a plastic ruler (Helix, England). Micrographs were not inverted between fiber imaging and diffraction analysis. Objects of known handedness were transformed, to insure that the transform was not inverted relative to the object in the microscope. Because of the nonlinearities of the video camera, the transforms should be considered as rapid, high quality analogues to optical diffraction.

Mass Measurements

Absolute particle masses were determined by the techniques developed by Wall and collaborators (Lamvik and Langmore, 1977; Wall et al., 1979). Data were recorded and analyzed using the Brookhaven National Laboratory STEM (Mosesson et al., 1981; Hainfeld et al., 1982). Chromatin samples were fixed in EB with 0.5% glutaraldehyde for 24 h at 0°C, injected into a drop of 100 mM ammonium acetate on a fresh carbon film, incubated for 2–4 min, washed with twelve drops of 100 mM ammonium acetate, freeze-dried overnight, and examined at 40 KeV at −160°C. Less than 3% mass error was caused by the imaging dosage of 250 electrons/nm^2 (our data, unpublished). Scattering from straight, uniform fibers was measured and converted to daltons using the internal mass standards of TMV (131,300 daltons/nm; Caspar, 1967), and oligonucleosomes (assumed to be multiples of 267,000 and 296,000 daltons for *Necturus* and *Thyone*).

RESULTS

Isolation of Chromatin Without Disruption

We have previously shown that intact nuclei could be isolated from erythrocytes and sperm using buffer MB (Langmore and Paulson, 1983). Fig. 3 confirms that intact soluble chromatin fibers can be prepared from *Necturus* erythrocytes. The diffraction patterns from nuclei isolated in MB and EB have common peaks at $1/s \approx 11$ and 6 nm because of similar internal fiber structure. The MB sample exhibited a reflection at $1/s \approx 35$ nm, because of the side-by-side packing of the fibers characteristic of nuclei in the presence of divalent cations (Langmore and Paulson, 1983). As expected from previous electron microscopy and x-ray studies, nuclei in EB had neither chromatin bodies nor a packing reflection. Nuclease digestion of the nuclei under conditions of no proteolysis resulted in obliteration of the $1/s \approx 35$, 20, 11, and 6 nm features, showing that the reflections originated from chromatin and not other cellular structure. The diffraction patterns from isolated fibers in EB were very similar to those of nuclei, showing that extraction of chromatin in 5 mM EDTA did not significantly alter chromatin structure. In contrast, extraction in 0.2 mM EDTA (as used by many other investigators) apparently prevents the full recovery of regular structure in EB, as evidenced by a marked degradation in the diffraction contrast (data not shown).

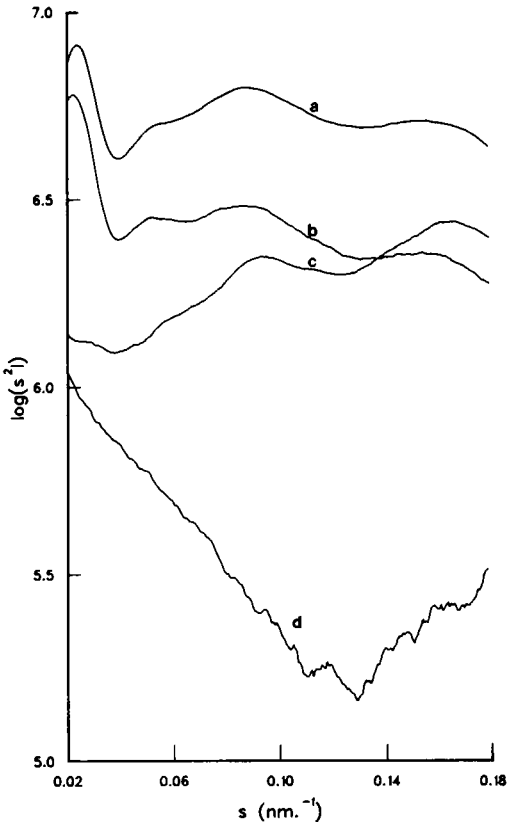

FIGURE 3 Comparison of x-ray scattering profiles from *Necturus* chromatin. (*a*) Isolated chromatin in EB; (*b*) nuclei in EB; (*c*) nuclei in MB; and (*d*) DNAse I-digested nuclei in EB after high salt treatment. The patterns from nuclei are presented as absolute intensities, scaled to a constant concentration of nuclei, taking into account x-ray absorption and beam intensity. The scattering from isolated fibers is scaled arbitrarily. The background scattering from nonchromatin structure is obviously negligible.

X-ray Diffraction of Chromatin with Different Repeat Lengths

The linker length is one of the few parameters of chromatin structure that can be independently varied. Because the dependence of fiber diameter upon linker length is a distinguishing characteristic of the models, we studied x-ray scattering from seven types of nuclei under identical conditions, taking care to inhibit both the serine and sulfhydryl proteases. Fig. 4 shows that the differences in diffraction are most evident in the region ~20 nm. *Necturus* and *Thyone* nuclei diffract strongly at 19.7 nm and 24.6 nm, whereas chicken erythrocytes diffract weakly at 20.2 nm. The features at 11, 6, 3.8, and 2.7 nm are conserved, presumably as the result of conserved interac-

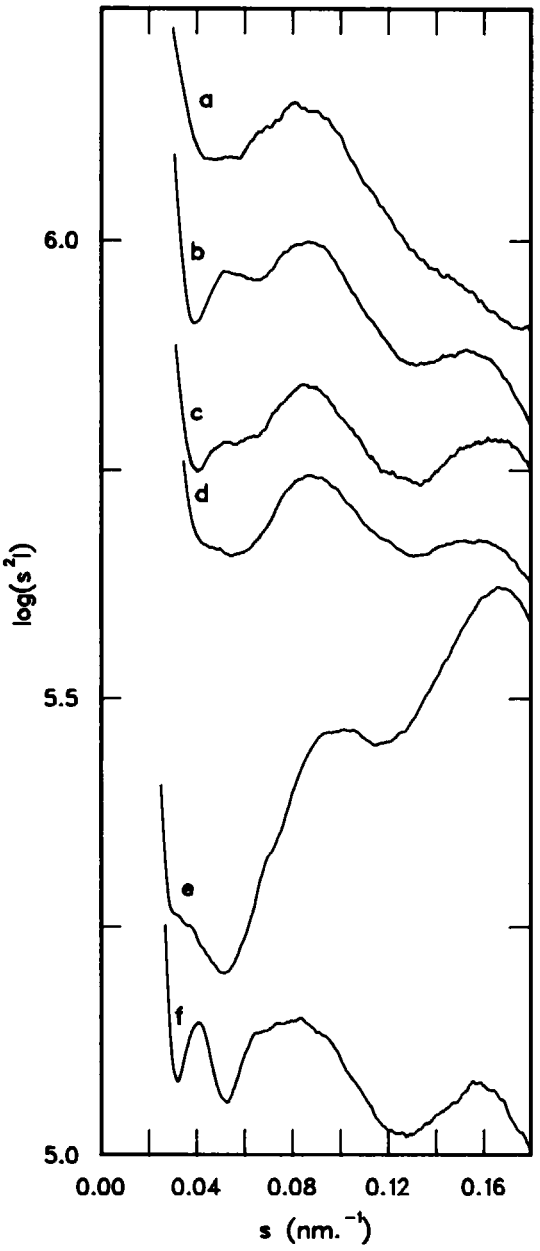

FIGURE 4 X-ray diffraction profiles of different chromosome fibers in EB. (*a*) Mouse myeloma nuclei; (*b*) *Necturus* erythrocyte nuclei; (*c*) *Xenopus* erythrocyte nuclei; (*d*) chicken erythrocyte nuclei; (*e*) isolated *Pisaster* sperm chromatin; and (*f*) *Thyone* sperm nuclei. *Pisaster* chromatin was extracted before study, because of many nonchromosomal peaks in the scattering from intact nuclei.

tions among the nucleosomes (Langmore and Paulson, 1983).

The "20 nm" feature has been attributed to the helical pitch (e.g., Perez-Grau et al., 1984), or to the fiber diameter (e.g., Langmore and Paulson, 1983). In the former case, the scattering should be almost meridional (along the fiber axis). In the latter case the scattering should be equatorial (perpendicular to the fiber axis). Low-angle equatorial diffraction from uniform cylindrical objects is described by a zeroth order Bessel function with a first subsidiary maximum of radius inversely proportional to the fiber diameter and insensitive to internal structure (Oster and Riley, 1952). If the "20 nm" reflections were equatorial, their positions would be directly related to the fiber diameters within intact nuclei. Because the diffraction patterns are unoriented, we cannot directly test whether that is the case. We can, however, test whether the "20 nm" reflections are modulated, as expected, by other equatorial functions such as the lattice interference due to side-by-side packing of the fibers in MB. Indeed, the scattering at ~20 nm is less in MB than in EB (Fig. 3), in agreement with expectations for an equatorial reflection. Thus, there should be a direct relationship between the position of the reflection and the fiber diameter.

Assuming that the "20 nm" feature was due to the scattering of the fibers as cylinders, we modeled the intensity and position of the reflection to determine the diameter of the fibers. Fig. 5 compares the experimental scattering from *Thyone* sperm nuclei to the calculated scattering from cylinders 39.4 nm in diameter. The fit is satisfactory over the expected limited range of *s*. Similar fitting was performed to determine the diameter of chromatin fibers with different linker length.

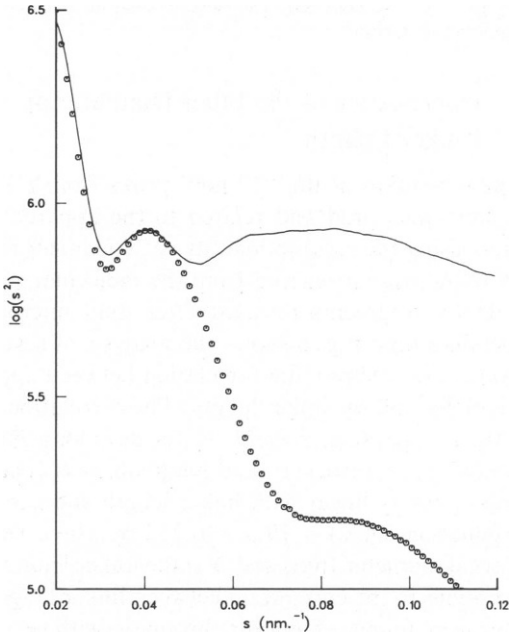

FIGURE 5 Comparison of predicted and observed low angle x-ray scattering. Observed scattering (—) is from *Thyone* sperm nuclei in EB. Calculated scattering (· · ·) is from a gaussian distribution of cylinders with mean outer diameter of 39.4 nm, mean inner diameter of 7.8 nm, and a standard deviation of 22%. The fitting procedure is described in Methods. The fit is over a narrow range of *s* due to contributions from interparticle interference at very low *s*, and contributions from intraparticle interference at higher *s*. The position of the calculated peak is determined by the outer diameter of the fibers. The other parameters of the fit are only used to maximize the fit over the largest angular range. Similar fitting could be achieved by introducing other parameters such as background scattering, fiber curvature, or internal structure. Thus there is no direct evidence that the fibers are hollow or are of heterogeneous width.

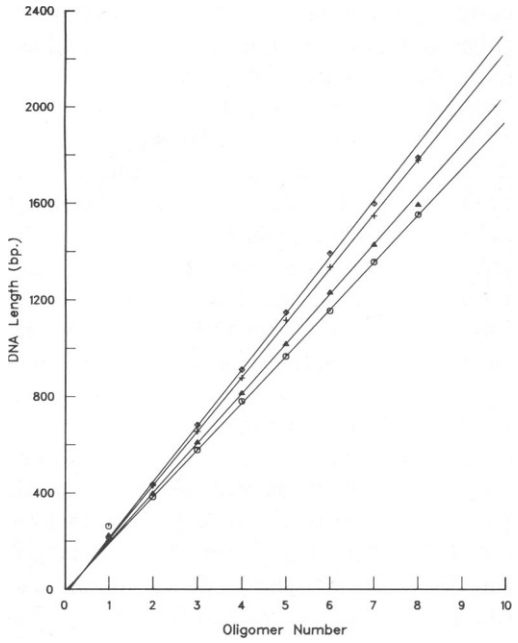

FIGURE 6 Four examples of nucleosome repeat length determinations. The number of base pairs in the fragment was plotted vs. number of nucleosomes in the fragment for *Thyone*, (□); *Pisaster*, (+ + +); *Necturus*, (Δ); and myeloma cells (○). The slope of each line is equal to the nucleosome repeat length.

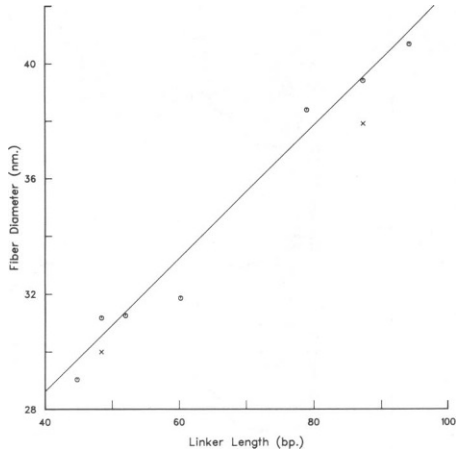

FIGURE 7 Correlation of the linker lengths with the fiber diameters determined from the position of the 20 nm feature in the x-ray patterns of nuclei in EB (○), and from electron microscopy of negatively stained isolated fibers fixed in EB (x). For the different samples, the linker lengths and apparent fiber diameters from x-ray data are: mouse (45 bp, 29.0 nm); *Necturus* (48 bp, 31.2 nm); *Xenopus* (52 bp, 31.3 nm); chicken (60 bp, 31.9 nm); *Pisaster* (79 bp, 38.4 nm); *Thyone* (87 bp, 39.4 nm); and *Strongylocentrotus* (94 bp, 40.7 nm). Analysis of the electron images gave mean diameters of 30 nm for *Necturus* and 37.9 nm for *Thyone*.

Dependence of the Fiber Diameter on Linker Length

The actual position of the "20 nm" peaks from all seven tissues were measured and related to the apparent fiber diameters using the assumptions above. The linker lengths of each tissue were measured from the molecular weights of the DNA fragments released after mild micrococcal nuclease digestion. Fig. 6 shows the analysis of several of the tissues. Fig. 7 shows the correlation between apparent fiber diameter and the linker length. The correlation exists within tissue-types (e.g., sperm), as well as among different tissues (sperm, erythrocytes, and lymphoblasts). The fiber diameter is nearly linear with linker length and can be fit by the equation: $D(N) = 19.3 + 0.232\,N$, where $D(N)$ is the external diameter (nm) and N is the linker length (bp). No exceptions to the correlation between linker length and diameter were found, except for chromatin with very short linkers (i.e., *Tetrahymena* and CHO), which did not have sufficient contrast to identify the 20, 11, or 6 nm reflections. We cannot conclude, however, that short-linker chromatin cannot form higher order structures, especially in view of the microscopic and hydrodynamic evidence of thick fibers (Rattner et al., 1982; Pearson et al., 1983; Allen et al., 1984).

To be certain that the "20 nm" feature was related to fiber diameter, the diameters of negatively stained *Necturus* and *Thyone* fibers were also measured by microscopy. The qualitative difference in these fiber diameters is apparent in micrographs (Fig. 8). Histograms of the measurements (Fig. 9) demonstrate that the fiber diameters are distinguishable, and quantitatively related to the diameters derived from x-ray scattering (Fig. 7). Unstained freeze-dried fibers were measured in STEM images and found to have diameters that were only 4% less than those in negative stain (data not shown).

Mass per Unit Length of Chromatin Fibers

The chromatin fibers used for mass analysis in the STEM were chosen to be long and straight. The fibers that were partially unraveled or contained particulate dislocations had low mass per unit length values that were not included in our analysis. Using the scattering from the TMV internal standard, the linear mass densities of *Necturus* and *Thyone* fibers were determined to be 232,000 ± 39,000 and 375,000 ± 60,000 daltons/nm (Fig. 10). To avoid potential systematic errors resulting from salt binding, mass loss, or fixation, we also determined the apparent nucleosome masses by measuring the scattering from nucleosome oligomers within the same specimens. The measured repeat unit masses were 315,000 ± 40,000 daltons for both *Necturus* and *Thyone*, ~10% larger than expected. Using 315,000 daltons as the effective mass of a nucleosome, the linear density of nucleosomes along *Necturus* and *Thyone* fibers was determined to be 7.4 ± 0.9 and 11.9 ± 1.9 nucleosomes/10 nm.

Helical Symmetry of the Fibers

Fourier transforms of the images of negatively stained fibers from *Necturus* and *Thyone* demonstrate that the fibers are helical. Fig. 11 *a* shows the transform of a slightly stretched *Necturus* fiber under conditions where

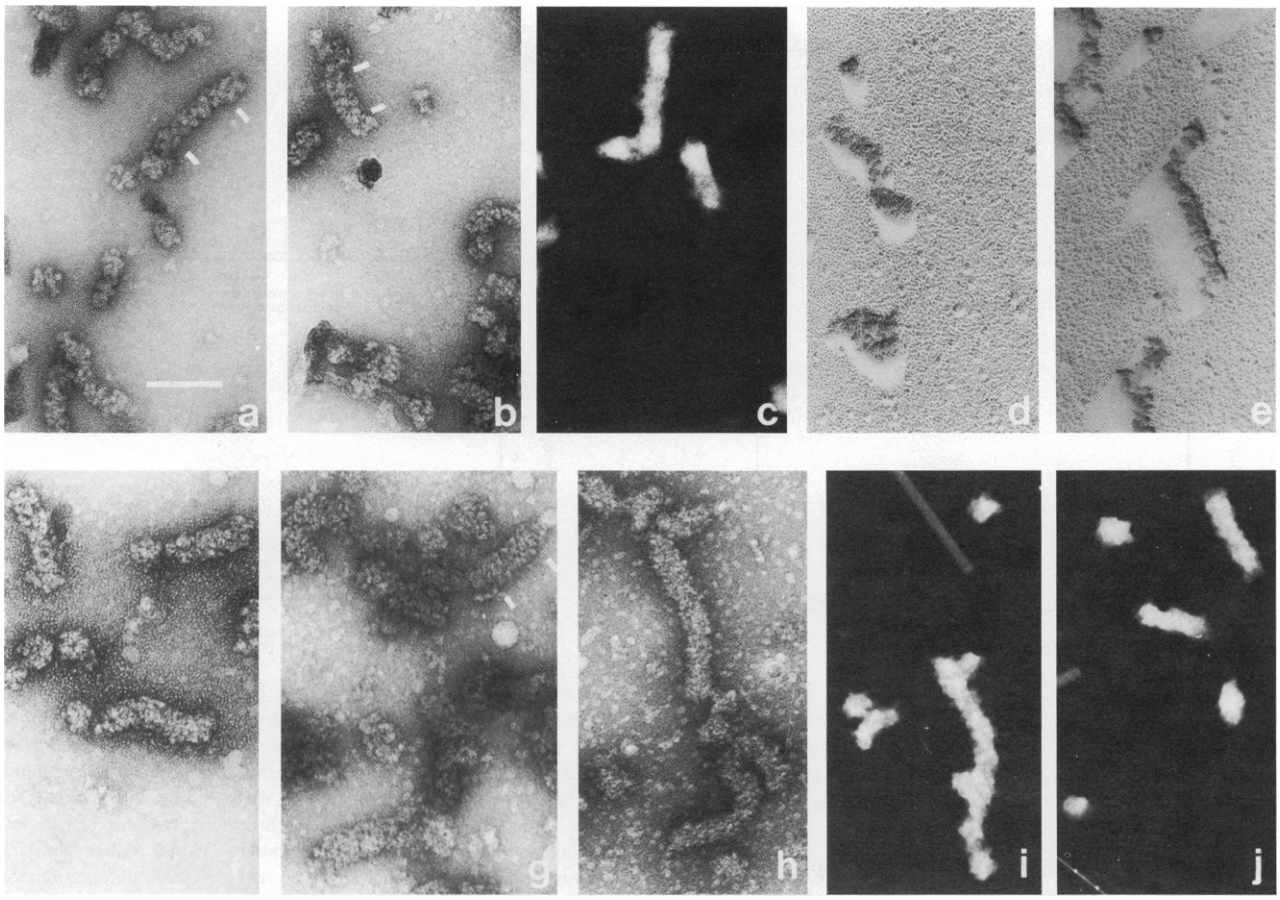

FIGURE 8 Electron micrographs of chromatin fibers from *Necturus* erythrocytes (*a–e*) and *Thyone* sperm (*f–j*). *a, b, f,* and *g* were negatively stained with uranyl acetate; *h* was negatively stained with 2% silicotungstic acid; *c, i,* and *j* were unstained and viewed in the STEM; *d* and *e* were unidirectionally shadowed. The micrographs (with the exception of *d* and *e*) were printed so that the side of the fiber closest to the carbon film (the near side) is facing up. The left-handed ramps are visible, especially in panels *b, d, e,* and *f*. The straight rods seen in the STEM images are the TMV particles used for mass calibration. The white bars delimit regions of the fibers that were used for the Fourier transforms shown in Fig. 11. The horizontal scale bar represents 100 nm.

both sides of the fiber have become stained. The characteristic cross pattern of helical order is apparent. In most cases (e.g., Fig. 11 *b,c*) the Fourier transforms show intensity on only one side of the meridian, presumably because the stain contrasted only one side of the helix. The average layer line spacings were 12.9 ± 0.4 nm for *Necturus* and 13.9 ± 1.7 nm for *Thyone*. When the microscope grids were oriented specimen-side-down, the strongest computed diffraction features were observed at $\alpha = 32 \pm 3°$ clockwise from the meridian in *Necturus*, and $\alpha = 23 \pm 7°$ clockwise in *Thyone*. If we assume that the negative stain contrasted helical ramps on the "near" side of the fibers (Klug and Berger, 1964), these off-meridional features consistently indicated left-handed helices.

To confirm the handedness, the front side of metal-shadowed *Necturus* fibers were directly imaged, with the result that 90% of the 49 shadowed fibers exhibiting helical ramps were left-handed (see Fig. 8 *d,e*). Thus the transforms of the negatively stained and the shadowed fibers are only consistent with left-handed helical models for chromatin.

The three classes of helical structure can be distinguished on the basis of the helical pitch, p, and the number of equivalent ramps per helical repeat, n. Solenoid models possess a single helical ramp ($n = 1$), and a pitch of ~11 nm that is independent of linker length. Twisted-ribbon models have one helical ramp ($n = 1$), composed of the ribbon of dinucleosomes, and variable pitch. The crossed-linker models should have ~13 nm between helical gyres, and therefore a pitch of about n times 13 nm.

From model building, we predict that the twisted-ribbon models would have layer lines at multiples of $1/s \approx$ 32 nm for *Necturus* and ≈39 nm for *Thyone*. The observed layer lines at 12.8 nm and 13.7 nm do not meet these expectations. The conserved maximum at $1/s \approx 11$ nm in the x-ray scattering patterns is also inconsistent with the variable pitch predicted by the twisted-ribbon model. We conclude that the twisted-ribbon models are not compatible with our microscopy or x-ray scattering results.

We can test whether the empirical values for p and α are consistent with $n = 1$, 2, or 3. We know the position of the maximum of the nth order Bessel function of the first kind

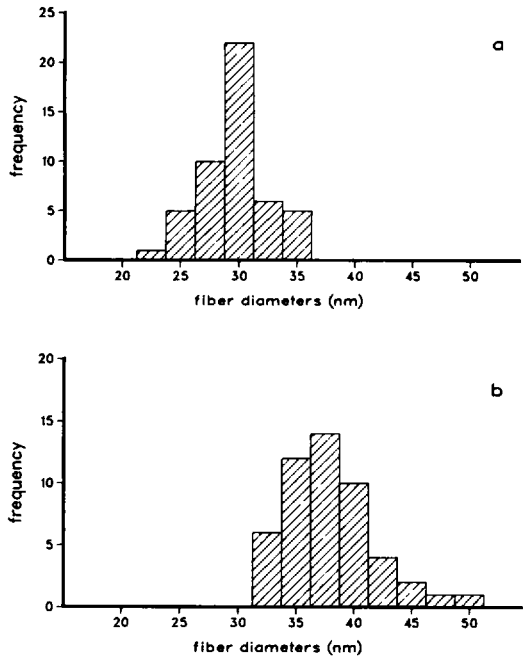

FIGURE 9 Histograms of chromatin fiber diameters determined from conventional electron microscopy of chromatin fixed in EB and negatively stained with uranyl acetate. (*a*) *Necturus* erythrocyte chromatin (mean diameter, 30.0 nm; standard deviation, 3.13 nm). (*b*) *Thyone* sperm chromatin (mean diameter, 37.8 nm; standard deviation, 3.78 nm).

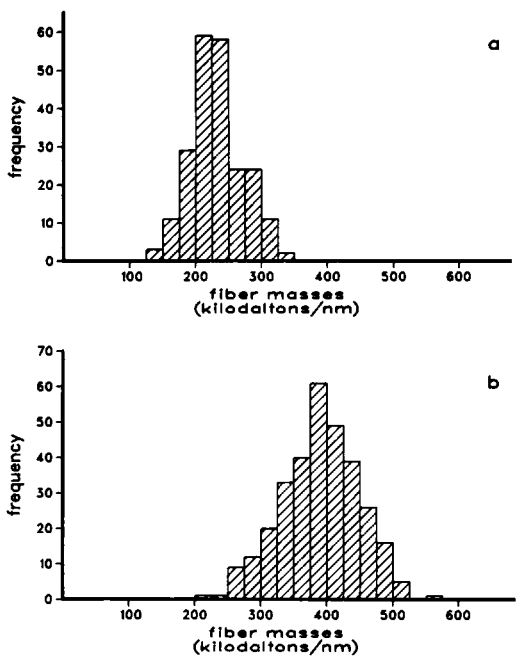

FIGURE 10 Histograms of chromatin fiber mass per unit length determined from scanning transmission electron microscopy of chromatin fixed in EB and examined unstained. The mass values shown were calculated using TMV as the mass standard. To convert these values to number of nucleosomes per unit length, we used the empirical nucleosome mass of 315 kd. (*a*) *Necturus* erythrocyte chromatin (mean mass, 232,000 daltons/nm; standard deviation, 39,000 daltons/nm). (*b*) *Thyone* erythrocyte chromatin (mean mass, 375,000 daltons/nm; standard deviation, 60,000 daltons/nm).

that is expected on the layer line, in terms of p, α, and r, the effective radius of the fibers. We cannot predict the value of r exactly, because we do not know how far the negative stain penetrates into the fiber. The most reasonable value for r is the radius to the center of the nucleosomes (i.e., r = 9.5 nm for *Necturus* and 13.5 for *Thyone*, assuming external diameters given by electron microscopy, and a nucleosome diameter of 11 nm). Incomplete penetration of stain would increase the expected values of r. Based on the experimental values of p and α for *Necturus*, the effective radii of stain contrast were calculated to be 6.1 nm, 10.0 nm, and 13.8 nm for n = 1, 2, and 3. The effective radii for *Thyone* (which were less reliable than those for *Necturus* because of greater variance of p and α) were calculated to be 10.0 nm, 16.5 nm, and 22.7 nm for n = 1, 2, and 3. Thus, the calculated values of r for n = 1 are too small, and the calculated values of r for n = 3 are too large to fit the data. The values of r for n = 2 fit our expectations. We conclude that chromatin fibers are neither single- nor triple-helices.

DISCUSSION

There are obvious model-independent conclusions to be drawn from the data presented. The diameter of chromatin fibers increases linearly with linker length. Also the number of nucleosomes per unit length increases with increasing amounts of linker DNA. The chromatin fibers have left-handed helical symmetry, with two equivalent ramps in the helical repeat.

Information from the observed Fourier transforms can be combined with the data on the external geometry of the fibers in order to make statements about specific models that have been proposed for chromatin structure. Our data exclude the solenoid, twisted-ribbon, and supranucleosomal particle models, as well as crossed-linker models with n = 1 or 3.

Chromatin Fiber Diameter

Our conclusions about the relationship between fiber diameter and linker length were derived from analysis of the structure of chromatin from tissues with different average linker lengths. Thus, these conclusions are important constraints on models for the static structure of chromatin, and the tissue-specificity of that structure. We also expect, however, that our conclusions are relevant to the heterogeneity of chromatin structure within individual cells.

Previous to our results, there had been no evidence of any differences in fiber diameter, primarily because other x-ray and electron microscopic investigations had been limited to one tissue at a time, and because the comparative studies of the hydrodynamic parameters such as rotational relaxation times and sedimentation coefficients (e.g., McGhee et al., 1983; Butler, 1984) were too insensitive to detect the observed differences.

We feel confident about the relationship between fiber diameter and linker length because of the excellent correla-

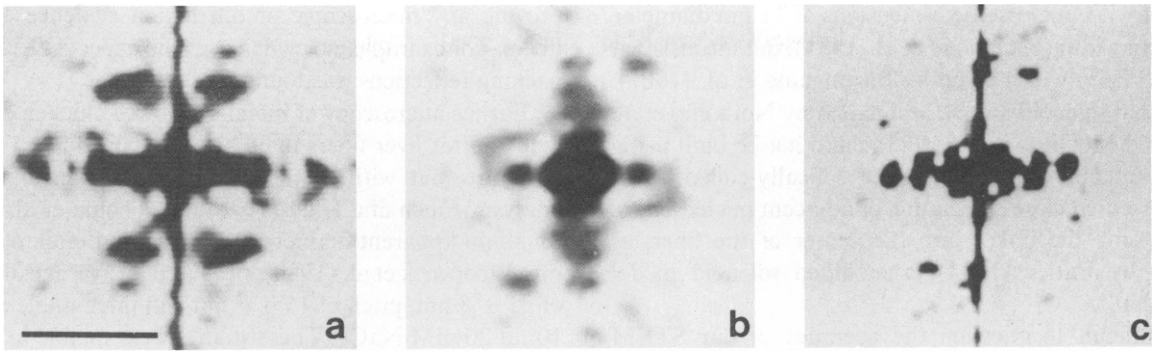

FIGURE 11 Fourier transforms of electron micrographs of negatively stained chromatin fibers. (*a*) Transform of a *Necturus* fiber (Fig. 7 *a*), showing the "cross" expected from a fiber stained on the front and back sides. This fiber is obviously stretched, because it has an atypical diameter (26 nm), and layer line spacing (16.9 mm). (*b*) Transform of a *Nectarus* fiber (Fig. 7 *b*), showing equatorial reflections at $1/s$ = 22.6 nm, and off-meridional features at an angle of 29°, on an apparent layer line at $1/s$ = 12.6 nm. (*c*) Transform of a *Thyone* fiber, showing off-meridional features at an angle of 27°, on an apparent layer line at $1/s$ = 13.6 nm. The orientation of the features indicates left-handed helical ramps.

tion between the results of electron microscopy and x-ray scattering; the controlled circumstances of preparation procedure, data collection, and data analysis; and our use of physiological concentrations of monovalent salt. Our absolute values of fiber diameter are in good agreement with neutron scattering in solution (Suau et al., 1979). Furthermore, the fiber diameters are not sensitive to ionic strength, as indicated by the radius of gyration measurements of Suau et al. (1979), and our x-ray measurements showing less than a 5% change in the Necturus fiber diameter between 75 and 150 mM monovalent salt (unpublished data).

Because of the lack of earlier evidence of fiber variations, most investigators have maintained that the solenoid and twisted-ribbon models require a fixed external geometry (e.g., McGhee et al., 1983; Woodcock et al., 1984; Butler, 1984). Not only is that constraint incorrect, but also unnecessary for the solenoid and twisted-ribbon models, which can accommodate variations in the diameter. Only the crossed-linker models are constrained to particular diameters and dependence of the diameters upon linker length. Although our diameter data agree with the very specific predictions of the crossed-linker models, they are not inconsistent with the less specific predictions of other helical models.

The external geometry of fibers might also vary within a tissue, owing to the well-studied heterogeneities in linker length within a tissue (Prunell and Kornberg, 1982). This heterogeneity has structural consequences for all classes of chromatin models. We have indirect evidence of this effect in chicken erythrocyte chromatin, which has a heterogeneous linker length (e.g. Compton, et al., 1976) and seems to have a heterogeneous diameter, as evidenced by a very weak 20 nm reflection. This heterogeneity in diameter (and linker length) might be related to the complexity of the very-lysine-rich histones of avian erythrocytes. Chicken erythrocytes have three major very-lysine-rich proteins (as detected by SDS-polyacrylamide gel electrophoresis) including the erythrocyte-specific histone, H5. In contrast, amphibian erythrocyte chromatin is more uniform in diameter, and has only one major and one minor electrophoretic form of very-lysine-rich histone, neither being erythrocyte-specific (Brown et al., 1981; Risley and Eckhardt, 1981; Shimada et al., 1981; our results, unpublished). In addition, *Thyone* and *Pisaster* sperm chromatin, which also have uniform diameters, contain only one major electrophoretic species of very-lysine-rich histone (our results, unpublished). Studies of another sea cucumber in the same family as *Thyone* have shown that the somatic and sperm histones are identical, and that the very-lysine-rich histone is antigenically related to calf thymus H1 (Subirana, 1970; Martinez and Palau, 1982).

Mass per Unit Length of Chromatin Fibers

The mass per unit length is an important detail of chromatin structure. However, none of the classes of chromatin structure can be proven to be correct or incorrect based on mass data alone. Any valid detailed model for chromatin must take into account the experimental mass per unit length, as well as the evidence from neutron scattering, hydrodynamics, and microscopy that the mass per unit length is quite variable, depending on ionic conditions (e.g., Suau et al., 1979; McGhee et al., 1983; Woodcock et al., 1984).

Ours were the first comparative measurements of the mass per unit length of chromatin fibers. Even though our analysis was limited to only two tissues, we expect that the linear mass density of all fibers will depend upon fiber diameter (and thus linker length), as a consequence of conserved interactions among nucleosomes.

Space-filling models demonstrated that the twisted-ribbon and crossed-linker structures can be built using the experimental values for mass and diameter (e.g., Fig. 1 *d*; and 2 *d*, *f*). These data dictate tight packing of nucleosomes (~7.4 nm between the centers of adjacent subunits),

consistent with nucleosome dimensions of 11 nm diameter and 5.7 nm width (Richmond et al., 1984), but inconsistent with the 11 nm width given by Burlingame et al. (1985). The original solenoid model, as detailed by Notbohm et al. (1979) and McGhee et al. (1983) could not be built using the experimental data because the helically-coiled linker DNA prevented close association of adjacent nucleosomes. By displacing the linker into the center of the fiber, as proposed by Butler (1984), a modified solenoid model could be built.

It is difficult to question the accuracy of our STEM measurements, because we used two independent internal standards for purposes of calibration and control for the effects of mass loss, salt binding, fixation, etc. The independent STEM results of Woodcock et al. (1984) at 100 mM NaCl indicated ~7.4 nucleosomes/10 nm for chicken erythrocyte fibers, which is not significantly different from our predictions for chicken.

It is difficult to reconcile our results with the values of 6 ± 1 nucleosomes/11 nm derived from hydrodynamic data (McGhee et al., 1983; Butler, 1984), light scattering (Campbell et al., 1978) and neutron scattering (Suau et al., 1979). For example, the rotational relaxation times predicted from our data are ~40% lower than the measurements of McGhee et al. (1983) for chicken erythrocytes.

Several factors might have contributed to these discrepancies. We studied fibers from *Necturus* and *Thyone*, which we believe are more uniform than those from other tissues (especially chicken erythrocytes), as evidenced by stronger diffraction at ~20 nm. In addition, the fibers were selected to have high axial ratios and uniform diameters—characteristics of the fibers that gave good Fourier transforms. The average fiber chosen for mass analysis contained ~100 nucleosomes, thus minimizing "end-effects." In addition, we took care to insure preservation of the fibers, as judged by x-ray scattering. This required (*a*) the use of physiological monovalent salt concentrations; (*b*) inhibition of both the serine and thiol proteases; and (*c*) fixation of the chromatin under mild conditions (Langmore and Paulson, 1983). Most other data have been collected at reduced ionic strength, where there is sound evidence of a lower mass-per-unit length (Suau et al., 1979; Butler and Thomas, 1980; McGhee et al., 1983; Woodcock et al., 1984).

Helical Nature of Chromatin Structure

Evidence of helical structure has been reported earlier by other investigators. Partially oriented x-ray patterns have been recorded from H1-depleted and intact chromatin after partial dehydration (Carpenter et al., 1976; Baldwin et al., 1978; Azorin et al., 1980). These patterns showed weak features ~8° from the meridian at a spacing of $1/s$ = 8.7 nm, which were interpreted to support a solenoid model. It is difficult to evaluate these data, however, because H1-depleted chromatin is not thought to form thick fibers (Thoma et al., 1979) and the authors did not provide any microscopic or diffraction evidence of thick fibers. For example, no evidence of the expected equatorial packing reflections was found.

Earlier microscopy of metal-shadowed chicken erythrocyte and rat liver fibers indicated the helical nature of the structure, but without the critical evaluation of Fourier analysis. Finch and Klug (1976) and Thoma et al. (1979) found an apparent diameter of 25 nm and pitch of 11–15 nm. Woodcock et al. (1984) measured an average diameter of 31 ± 8 nm, pitch of 15 ± 5 nm and pitch angle of 25 ± 10° at 20 mM NaCl. These studies were unable to resolve the handedness of the structure, although left-handed ramps were observed slightly more frequently than right-handed ramps (Thoma et al., 1979).

The Fourier transforms shown in Results are the first objective microscopic evidence that chromatin fibers are helical. The helical parameters are different for fibers from *Necturus* and *Thyone*, but reasonably consistent for different fibers from the same tissue. The observed values for p and α predict features in the x-ray patterns of randomly oriented fibers at $1/s$ = 10.9 nm for *Necturus* and 12.7 nm for *Thyone*, in agreement with our x-ray data, particularly that the "11 nm" peak in *Thyone* showed broadening toward smaller angles. Our values for the pitch (26–27 nm) are considerably larger than those derived by others, primarily because they interpreted the 11 nm x-ray peak as the first-order Bessel function on the first layer line of a single-start helix. We interpret that peak as the second-order Bessel function on the second layer line, based on the experimental fiber diameters and pitch angles, which are consistent with a left-handed double-helical structure. Combining our values for the mass-per-unit length with the values for the helical pitch, we conclude that *Necturus* fibers have 19 ± 3 and *Thyone* fibers have 33 ± 6 nucleosomes per helical repeat.

Evaluation of the Supranucleosomal Particle Model for Chromatin Fiber Structure

The observed Fourier transforms showed a definite helical organization to chromatin fibers. From the vertical spread of intensities on the second layer line (Fig. 11), it is estimated that the helical domains are at least 100 nm long—two or three times longer and containing up to 10 times more nucleosomes than the proposed supranucleosomal particles. We believe that the observations of particulate features in the fibers represent dislocations in the helix (modeled in Fig. 1 *e*) due to displacements of histones by natural or artificial means. Zentgraf and Franke (1984) measured different widths for chromatin particles from three different tissues (32 nm for liver, N = 50 bp; 36 nm for chicken erythrocytes, N = 60 bp; and 48 nm for sea urchin sperm, N = 95 bp), which they interpreted as differentiation-specific variations in the structure of supranucleosomal particles. We attribute their observa-

tions to linker-length–specific variations in the diameter of very short fibers.

Evaluation of the Double-Helical Crossed-linker Models for Chromatin Structure

The crossed-linker models are built from extended ribbons of nucleosomes (Fig. 2 *a, b*), which closely resemble the zig-zag structures seen in by microscopy of chromatin fibers at low ionic strength (e.g. Thoma et al., 1979; Worcel et al., 1981). To generate the double helices, the extended ribbons must be twisted about the long axis to give a left-handed helical sense, and compacted along the axis to increase the mass per unit length. In the case of chromatin having N = 48 bp, shown in Fig. 2 *a–f*, the ribbon was twisted 20° per nucleosome, and compacted by a factor of four. The resulting double-helical models have nearly maximal compaction, and have 26-nm pitch and 18 nucleosomes per turn—in good agreement with our experimental data. Neighboring nucleosome cores are closely spaced by about 4 nm at their inside edges. The 31–33 nm diameters of the models is nearly independent of the degree of compaction—in excellent agreement with the measured diameters and the dependence of the diameters and radii of gyration upon ionic strength.

Although the extended ribbons with $\Delta L = -1$ and -2 are distinguishable (Fig. 2 *a,b*), the corresponding double-helical fibers have the same external arrangement of nucleosomes (Fig. 2 *d,e*). The odd-numbered nucleosomes sequentially form one helical ramp, while the even-numbered nucleosomes sequentially form a second ramp in the opposite direction, as labeled in Fig. 2 *c* and *e*. The long axes of the nucleosome cores are oriented nearly parallel to the helical axis to fit the experimentally determined pitch and mass per unit length, and also to agree with the linear dichroism measurements of McGhee et al. (1983). The experimentally determined linear dichroism and linking number should be sensitive to small changes in the nucleosome tilt angle. However, we have not constrained the model to exactly fit those data due to uncertainties in their accuracy. We do note, however, that folding the extended ribbons into the cross-linker models shown in Fig. 2 *c–f* changes the linking number increments by an insignificant amount (-0.05).

The helical symmetry of the models depends on the number of nucleosomes per turn and nucleosome internal symmetry. The models shown in Fig. 2 *c–f* have an integral number of nucleosomes per turn and s2 helical symmetry. Thus, the two helical ramps are related by a twofold rotational axis perpendicular to the helical axis. This prevents the models from being polar. Assuming that the nucleosomes do not have twofold rotational symmetry (as in the case of only one molecule of H1 per nucleosome), the two helical ramps would be antiparallel.

The differences between the two topological variants are most evident in the path of the linker DNA within the structure. The linker DNA forms two smooth internal ladders, spaced by about 2.7 nm, center-to-center, and inclined at about 60° with respect to the fiber axis. Nucleosomal DNA diverges as it exists the core in the $\Delta L = -1$ structure (as seen in Fig. 2 *c*), resulting in a central home ~3 nm wide. Nucleosomal DNA converges as it exists the core in the $\Delta L = -2$ structure (as seen in Fig. 2 *e*), resulting in a more dense center and slightly smaller diameter. It is precisely the close fit of the linker DNA into two helical ladders that allows the left-handed models to be compacted to the experimental mass per unit length. Steric hinderance of the linker DNA prevents the construction of right-handed double-helical (as well as all single-helical) crossed-linker models that agree with the mass data.

Using the same local contacts among nucleosomes, as discussed above, a model built using the *Thyone* linker length has more nucleosomes per turn and greater diameter. This is in quantitative agreement with our structural data.

The model built using the chromatosome (Simpson, 1978), contains the minimum amount of linker DNA (N = 22 bp). From model building, it is found that only a ribbon with $\Delta L = -1$ per nucleosome allows a fiber to be made. The pitch of this structure is 30 nm, however, quite different from that we observe from *Necturus* and *Thyone*. If higher order structures can form from short linker chromatin (as reported by Rattner et al., 1982; Pearson et al., 1983; and Allen et al., 1984), it is likely that the $\Delta L = -1$ structure can exist in nature. This would be in agreement with the linking number measurements of Keller (1975) and Garguiluo and Worcel (1983), using short circular chromatin molecules. However, we don't want to discount the possibility that $\Delta L = -2$ structures exist, since electron microscopy indicates that chromatin at low ionic strength most closely resembles the $\Delta L = -2$ extended ribbons (e.g. Thoma et al. 1979; Woodcock et al., 1984), and x-ray diffraction indicates that the DNA converges as it exits from the nucleosome core (Richmond et al., 1984).

Yet, given the highly conserved nature of the nucleosome interactions in both topological variants, it is possible that both the $\Delta L = -1$ and -2 structures exist.

Assuming that the basic pattern of nucleosomes in the double-helical crossed-ribbon model is correct, nuclease digestion of adjacent nucleosomes on each ramp should preferentially release dinucleosomes, rather than mononucleosomes. This phenomenon has been seen after digestion of chromatin with immobilized DNAse I (Burgoyne and Skinner, 1982). In addition, because the path of the DNA between nucleosomes is from the top of one subunit to the bottom of the next, the linker length is quantified such that $N \approx 10\ m + 5$ bp, where m is an integer. This "reversed" arrangement of the nucleosomes has been proposed earlier, to explain the nuclease digestion patterns of yeast and rat

liver (Lohr and Van Holde, 1979; Strauss and Prunell, 1983). We think that the nuclease data is in strong agreement with the crossed-linker model.

Many aspects of the double-helical crossed-linker model have not yet been determined. For example, the exact number of nucleosomes per turn, the tilt of the nucleosomes, the actual linking number increment, and the location of histone H1 is not known. Clearly, further structural and biochemical experiments are needed to understand the structure and function of eukaryotic chromosomes.

We would like to thank K. Findling, E. Hurst, R. Barnisin, C. Cornell, D. Lee, and F. Guiffrida for laboratory assistance; L. Lutter, T. Baker, and J. Workman for many valuable discussions; J. Wall, J. Hainfeld, P. Kito, K. Chung, K. Monson, and P. Furcinitti for aid with STEM microscopy and mass analysis; and T. Connelly for use of the Zeiss SEM IPS, provided courtesy of Carl Zeiss, Inc.

These studies were supported by the National Institutes of Health (NIH) GM27937; the the Brookhaven STEM was supported by NIH grant RR 01777 and Department of Energy; B. D. Athey was supported by NIH predoctoral training grant T32 GM07315.

Received for publication 16 May 1985 and in revised form 1 July 1985.

REFERENCES

Allen, J., N. Harbourne, and H. Gould. 1984. Higher order structure in a short repeat length chromatin. *J. Cell Biol.* 98:1320–1327.

Allen, S. L., T. White, J. P. Langmore, and M. A. Swancutt. 1983. Highly purified micro- and macronuclei from *Tetrahymena thermophilia* isolated by Percoll gradients. *J. Protozool.* 30:21–30.

Azorin, F.,A. B. Martinez, and J. A. Subirana. 1980. Organization of nucleosomes and spacer DNA in chromatin fibres. *Int. J. Biol. Macromol.* 2:81–90.

Baldwin, J. P., B. G. Carpenter, H. Crespi, R. Hancock, R. M. Stephens, J. K. Simpson, and E. M. Bradbury. 1978. Neutron scattering from chromatin in relation to higher order structure. *J. Am. Chem. Soc.* 11:484–486.

Bates, D. L., P. J. G. Butler, E. G. Pearson, and J. O. Thomas. 1981. Stability of the higher order structure of chicken erythrocyte chromatin in solution. *Eur. J. Biochem.* 119:469–476.

Brown, G. L., R. G. Rutledge, and J. M. Neelin. 1981. Anuran erythrocytes and liver both contain satellite histone H1°. *Life Sci.* 28:2993–2999.

Burgoyne, L. A., and J. D. Skinner. 1982. Avian erythrocyte chromatin degradation: the progressive exposure of the dinucleosomal repeat by bovine-pancreatic-DNAase-I-armed probes and free DNAase-I. *Nucl. Acids Res.* 10:665–673.

Butler, P. J. G., and J. O. Thomas. 1980. Changes in chromatin folding in solution. *J. Mol. Biol.* 140:505–529.

Butler, P. J. G. 1984. A defined structure of the 30 nm chromatin fibre which accommodates different nucleosomal repeat lengths. *EMBO (Eur. Mol. Biol. Org.) J.* 3:2599–2604.

Campbell, A. M., R. I. Cotter, and J. F. Pardon. 1978. Light scattering measurements supporting helical structures for chromatin in solution. *Nucl. Acids Res.* 5:1571–1580.

Carpenter, B. G., J. P. Baldwin, E. M. Bradbury, and K. Ibel. 1976. Organization of subunits of chromatin. *Nucl. Acids Res.* 7:1739–1745.

Caspar, D. L. D. 1963. Assembly and stability of the tobacco mosaic virus particle. *In* Advances in Protein Chemistry. C. B. Anfinson, Jr., M. L. Anson, and J. T. Edsall, editors. Academic Press, Inc., New York. 37–121.

Chambers, S. A. M., J. P. Vaughn, and B. R. Shaw. 1983. Shortest nucleosomal repeat lengths during sea urchin development are found in two-cell embryos. *Biochemistry.* 22:5626–5631.

Compton, J. L., M. Bellard, and P. Chambon. 1976. Biochemical evidence of variability in the DNA repeat length in the chromatin of higher eukaryotes. *Proc. Natl. Acad. Sci. USA.* 73:4382–4386.

Davies, H. G. 1968. Electron-microscope observations on the organization of heterochromatin in certain cells. *J. Cell Sci.* 3:129–150.

Finch, J. T., and A. Klug. 1976. Solenoidal model for superstructure in chromatin. *Proc. Natl. Acad. Sci. USA.* 73:1897–1901.

Gall, J. G. 1963. Chromosome fibers from an interphase nucleus. *Science (Wash. DC.)* 139:120–121.

Gargiulo, G., and A. Worcel. 1983. Analysis of the chromatin assembled in germinal vesicles of *Xenopus* oocytes. *J. Mol. Biol.* 170:699–722.

Hainfeld, J. F., J. S. Wall, and E. J. Desmond. 1982. A small computer system for micrograph analysis. *Ultramicroscopy.* 8:263–270.

Igo-Kemenes, T., W. Horz, and H. G. Zachau. 1982. Chromatin. *Annu. Rev. Biochem.* 51:89–121.

Keller, W. 1975. Determination of the number of superhelical turns in simian virus 40 DNA by gel electrophoresis . *Proc. Natl. Acad. Sci. USA.* 72:4876–4881.

Klug, A., and J. E. Berger. 1964. An optical method for the analysis of periodicities in electron micrographs, and some observations on the mechanism of negative staining. *J. Mol. Biol.* 19:565–569.

Lamvik, M. K., and J. P. Langmore. 1978. Determination of particle mass using scanning transmission electron microscopy. *In* Scanning Electron Microscopy. O. Johari, editor. IIT Research Institute, Chicago. 401–409.

Langmore, J. P., and J. R. Paulson. 1983. Low angle x-ray diffraction studies of chromatin structure in vivo and in isolated nuclei and metaphase chromosomes. *J. Cell Biol.* 96:1120–1131.

Lohr, D., and K. E. Van Holde. 1979. Organization of spacer DNA in chromatin. *Proc. Natl. Acad. Sci. USA.* 76:6326–6330.

Makarov, V., S. Dimitrov, V. Smirnov, and I. Pashev. 1985. A triple helix model for the structure of chromatin fiber. *FEBS (Fed. Eur. Biochem. Soc.) Lett.* 181:357–361.

Martinez, P., and J. Palau. 1982. Antigenic variability among very-lysine-rich histones from calf thymus and from sperm of different echinoderms. *Comp. Biochem. Physiol.* 74B:611–617.

McGhee, J. D., and G. Felsenfeld. 1980. Nucleosome structure. *Annu. Rev. Biochem.* 49:1115–1156.

McGhee, J. D., J. M. Nickol, G. Felsenfeld, and D. C. Rao. 1983. Higher order structure of chromatin: orientation of nucleosomes within the 30 nm chromatin solenoid is independent of species and spacer length. *Cell.* 33:831–841.

Mosesson, M. W., J. Hainfeld, R. H. Haschemeyer, and J. Wall. 1981. Identification and mass analysis of human fibrinogen and its domains by scanning transmission electron microscopy. *J. Mol. Biol.* 153:695–718.

Notbohm, H., H. Hollandt, J. Meissner, and E. Harbers. 1979. Low angle x-ray scattering studies of chromatin in different solvents; analysis by comparison with computer-simulated scattering curves. *Int. J. Biol. Macromol.* 1:180–184.

Oster, G., and D. P. Riley. 1952. Scattering from cylindrically symmetric systems. *Acta. Crystallogr.* 5:272–279.

Pearson, E. C., P. J. G. Butler, and J. O. Thomas. 1983. Higher order structure of nucleosome oligomers from short repeat chromatin. *EMBO (Eur. Mol. Biol. Org.) J.* 2:1367–1372.

Perez-Grau, L., J. Bordas, and M. H. J. Koch. 1984. Chromatin superstructure: synchrotron radiation x-ray scattering study on solutions and gels. *Nucl. Acids Res.* 12:2987–2996.

Porod, G. 1948. Die Abhangigkeit der Röntgen-Kleinwinkelstreuung von Form und Grosse der kolloiden Teilchen in verdunten Systemen, IV. *Acta Phys. Aust.* 2:255–292.

Prunell, A., and R. D. Kornberg. 1981. Variable center-to-center distance of nucleosomes in chromatin. *J. Mol. Biol.* 154:515–523.

Rattner, J. B., C. Saunders, and J. R. Davie. 1982. Ultrastructure organization of yeast chromatin. *J. Cell Biol.* 93:217–222.

Renz, M., P. Nehls, and J. Hosier. 1977. Involvement of histone H1 in the

organization of the chromatin fiber. *Proc. Natl. Acad. Sci. USA.* 74:1879–1883.

Richmond, T. J., J. T. Finch, B. Rushton, D. Rhodes, and A. Klug. 1984. Structure of the nucleosome core particle at 7 Å resolution. *Nature* (*Lond.*). 311:532–537.

Risley, M. S., and R. A. Eckhardt. 1981. H1 histone variants in *Xenopus laevis*. *Dev. Biol.* 84:79–87.

Shimada, T., Y. Okihama, C. Murata, and R. Shukuya. 1981. Occurrence of H1°-like protein and protein A24 in the chromatin of bullfrog erythrocytes lacking histone 5. *J. Biol. Chem.* 256:10577–10582.

Simpson, R. T. 1978. Structure of the chromatosome, a chromatin particle containing 160 base pairs of DNA and all the histones. *Biochemistry.* 17:5524–5531.

Staynov, D. Z. 1983. Possible nucleosome arrangements in the higher-order structure of chromatin. *Int. J. Biol. Macromol.* 5:3–10.

Strauss, F., and A. Prunell. 1983. Organization of internucleosomal DNA in rat liver chromatin. *EMBO* (*Eur. Mol. Biol. Org.*) *J.* 2:51–56.

Suau, P., E. M. Bradbury, and J. P. Baldwin. 1979. Higher order structures of chromatin in solution. *Eur. J. Biochem.* 97:593–602.

Subirana, J. A. 1970. Nuclear proteins from a somatic and a germinal tissue of the echinoderm *Holothuria tubulosa*. *Exp. Cell Res.* 63:253–260.

Thoma, F., Th. Koller, and A. Klug. 1979. Involvement of histone H1 in the organization of the nucleosome and salt-dependent substructure of chromatin. *J. Cell Biol.* 83:403–427.

Tilney, L. 1976. The polymerization of actin II. How non-filamentous actin becomes non-randomly distributed in sperm. *J. Cell Biol.* 69:51–72.

Tomlin, S. G., and H. G. Callan. 1951. Preliminary account of an electron microscope study of chromosones from newt oocytes. *Quart. J. Microsc. Sci.* 92:221–224.

Wall, J. S. 1979. Biological scanning electron microscopy. *In* Introduction to Analytical Electron Microscopy. J. Hren, J. Goldstein, and D. Joy, editors. Plenum Publishing Corp., New York. 333–342.

Woodcock, C. L. F., L. L. Y. Frado, and J. B. Rattner. 1984. The higher order structure of chromatin: evidence for a helical ribbon arrangement. *J. Cell Biol.* 99:42–52.

Worcel, A., S. Strogatz, and D. Riley. 1981. Structure of chromatin and the linking number of DNA. *Proc. Natl. Acad. Sci. USA.* 78:1461–1465.

Workman, J. L., and J. P. Langmore. 1985. Efficient solubilization and partial purification of sea urchin histone genes as chromatin. *Biochemistry.* In press.

Zentgraf, H., and W. W. Franke. 1984. Differences of supranucleosomal organization in different kinds of chromatin: cell type specific globular subunits containing different numbers of nucleosomes. *J. Cell Biol.* 99:272–286.

DISCUSSION

Session Chairman: Lee Makowski
Scribes: Michael K. Reedy and Ayuko Yotsukara

WOOLEY: The Worcel and Woodcock twisted ribbon model (see references above) and your crossed linker model are derived from the zig-zag nature of chromatin observed at low ionic strength, whereas the Klug and Finch solenoid model (see references) depends on their observations of a 10 nm nucleofilament at low ionic strength. Could you comment on that discrepancy? What is your view of the structure of chromatin at low ionic strength?

LANGMORE: There seem to be differing observations of chromatin structure at low ionic strength. To my knowledge, John Finch is the only person who has observed a 10 nm nucleofilament. That observation was the basis for the solenoid model. Subsequent to his work, Worcel et al., Rather, and Hamkalo (*Chromosoma.* 69:363–372), Woodcock et al., and we have shown the zig-zag character to be intrinsic to the structure of chromatin at low ionic strength. Furthermore, chromatin adopts a zig-zag structure only in the presence of histone H1, which is known to be essential for the formation of higher-order structure. Solution studies by Suau et al. using neutron diffraction seem to indicate that during the folding process the radius of gyration is almost constant, whereas the mass per unit length increases dramatically. The crossed-linker model accounts for those observations and proposes a continuous transition between the unfolded and folded states. The solenoid model would have to fold in a discontinuous manner.

FRANK: I would like to mention that the 30 nm fiber was studied by Subirana and Frank (Subirana et al. 1985. *Chromosoma.* 91:377–390) and we did not find any evidence for such a helical arrangement. These were reconstructions of individual fibers. Ten fibers were reconstructed in three dimensions, but the resolution was just short of that necessary to distinguish nucleosomes. However, at our resolution we would definitely have observed a hollow core had one been present. We never observed one in any of the segments. So that piece of evidence would agree with your model.

LANGMORE: The neutron diffraction also argues against the hollow core. Our evidence that there is no hollow core comes partly from the electron micrographs of short *Thyone* and *Necturus* chromatin fragments that we believe lie face down on the grid. We believe that the slides just shown are end-on views of the fiber structure, because their diameters are the same as widths of the long fibers in the same micrographs. There appear to be nucleosome-size blobs in a circle, with space-filling material in the center. We can find numerous such images and we have image-processed some of them by power spectrum analyses and rotational averaging, using both optical and computer methods. The rotational averages show material in the center, as predicted by the cross-linker model. The solenoid and twisted ribbon models predict a large hole in the center. A computer power-spectrum analysis that I did in Nigel Unwin's laboratory consistently showed 10–13 blobs per turn in the *Thyone* end-on views, but only 6–9 blobs per turn in the *Necturus* end-on views. This is consistent with our findings that the mass per unit length and diameter of *Thyone* fibers are greater than those of *Necturus* fibers. Although the external geometry is quite variable, the actual spacing between the nucleosomes is very similar in all these structures.

BURNETT: How much signal do you recover in those processed images? Have you measured the power loss?

LANGMORE: These are by no means ideal images. The maximum power at any specific rotation was ~ 30%.

SALEMME: Have you ever computed the transform from your model and looked at how closely it corresponds to your observations?

LANGMORE: We are in the process of doing that. Although previously we could not get good x-ray patterns from short, linker-length chromatin, we have now found two short linker chromatins that give very good diffraction patterns. Those diffraction patterns are substantially different from the other tissues we have studied. Thus we will have the

opportunity to test our model for the pattern of folding against a spectrum of diffraction patterns observed from chromatin with very different linker lengths.

RUBEN: How do we know that the helicity of the sample is indeed left-handed? What precautions have you taken to insure that the orientation of the specimen and negative preserve the correct handedness?

LANGMORE: We have performed all the preparation and imaging steps with great care. We have excluded image inversion by relating the microscope stage motion to image motion. We have not found it necessary to include a reference structure of known hand with our specimens.

RUBEN: We find that the microscope simply spins the image (with no inversions). So if you have a metal-shadowed sample that is right-side-up, then the image should be viewed from the emulsion side of the negative in order to see the correct handedness.

LANGMORE: Our microscope operates in the same fashion.

STEWART: It seems to me that a critical difference between your model and many of the others is that it is two-stranded as opposed to one-stranded. Thus you are interpreting the principal reflection seen as a J_2 rather than a J_1 Bessel term. You have argued strongly for this reflection being a J_2 based on the radial position of its maximum in the Fourier transform. Of course this assumes that you know the radius of the particle in real space. It seems that the alternatives to a two-stranded model are one and three. I wonder, therefore, if you have examined the phase of these reflections, because there is a very different relationship in the odd and even cases.

LANGMORE: You are correct. If we had the phases of the two reflections on the double-sided patterns, we could tell immediately if we had an even or odd Bessel function. We do not have those image-processing capabilities yet, but soon will. The work I have shown today has been done on a video-based system that does not give us access to the phases.

STEWART: One of your slides showed two rotationally filtered images and it appeared that they are derived from two components, the J_5 and J_{10} Bessel terms. These give you the appearance of subunits at a radius of ~ 10 nm. In *Thyone*, for instance, ten subunits show up very clearly. This seems to me to be a very separate idea from showing that there is no hole down the center, which depends on your J_0 term. I wonder how well your model fits into the positions that you actually observe for subunits. If you put the center of a nucleosome at these positions, would half of the nucleosome go into the center so that you would have no hole? In other words, is the radius at which you find maximum six- and 10-fold power consistent with the radius you would expect from your model or is it consistent with the solenoid model?

LANGMORE: If we assume that the peripheral blobs are nucleosome cores, then there is a "space" devoid of nucleosome cores at the center of the *Thyone* images that has a diameter of at least 15 nm. In both the processed and unprocessed images, you can see material filling that "space." Thus, the end-on views are consistent only with the crossed-linker models.

STEWART: Do you really mean that there is no stain there?

LANGMORE: Yes. Something is excluding the stain. In our model, that "something" is linker DNA.

BLOOMFIELD: All of these models imply a more or less rigid, regular structure. An outsider might wonder whether the properties of DNA would allow a more flexible solenoid or helix. If so, the Finch and Klug model might not be ruled out because the central hole might be filled by relaxed segments of linker DNA. As your power spectrum gives only 30% recovery, there seems to be a lot of irregularity in the structure you are observing. At this level of analysis, what is your basis for assuming a rigid helical structure?

LANGMORE: The micrographs show straight regions of substantial length and uniform diameter. The contrast and width of the x-ray scattering peak at $1/s = 20$ nm show that the variation in fiber diameter is small. The finding of a helical diffraction pattern also argues for a regular structure.

BLOOMFIELD: All of these findings occur in environments where crystal packing or contact with the grid might reinforce any regularities present. But what do the structures look like in the cell?

LANGMORE: Normally, one expects specimen preparation for electron microscopy to destroy rather than reinforce sample periodicity. The diffraction patterns from specimens in solution are consistent with, but by no means prove, perfect helical symmetry. Everyone agrees that chromatin fibers must bend extensively within nucleii, thus distorting the helical symmetry.

MAKOWSKI: Let me summarize a question from a referee: In many chromatins, such as rat liver, there is a large variation in linker length. How do you accommodate such a variation with your observation of a regular ordering of the nucleosomes?

LANGMORE: We would predict that if linker length is heterogeneous, fiber diameters should vary as well. Different tissues exhibit varying degrees of contrast in the $1/s = 20$ nm peak. For example, chicken erythrocyte chromatin has almost no peak at this spacing. If the lack of contrast in this region indicates heterogeneity in the fiber diameter, as we believe, we expect great heterogeneity in the linker length in this tissue. The literature shows that chicken erythrocyte chromatin indeed has a very heterogeneous linker length. All chromatin is not created equally periodic. We tried for many years to get Fourier transforms of chicken erythrocyte chromatin that would show helical structure, but we failed. We were successful with tissues that gave better diffraction patterns and more uniform linker length.

BINA: In your modeling you have used the nucleosome structure as solved at MRC in Cambridge, England (Richmond et al., 1984. *Nature (Lond.)* 311:532–537). Can you construct an equivalent model using the nucleosome structure recently proposed in an article in *Science (U.S.A.)* by the Johns Hopkins group (Burlingame et al.)?

LANGMORE: If our mass-per-unit-length data and helical pitch data are as good as I believe they are, then the center-to-center distance between successive nucleosomes is ~ 6.5 nm. That distance is too close to accommodate the Hopkins model of Burlingame et al., but would be in agreement with the Cambridge model.

RAGHAVENDRA: Could you please elaborate further on how you determine the handedness from the fiber diffraction pattern?

LANGMORE: Because of the way we position both metal-shadowed and negative-stained specimens in the microscope, we believe we are seeing

the front side of this fiber in our micrographs. The front side of a left-handed helix shows helical ramps rotated clockwise from horizontal. Therefore, the transform of a left-handed helix shows the corresponding reflections rotated clockwise from the meridian. Thus, the Fourier transforms in Fig. 11 indicate left-handed symmetry.

FRANK: You postulated a thickness variation that would somehow account for the linker length variation. Could such a thickness variation explain superbead formation? How do you explain superbeads?

LANGMORE: A superbead is a cluster of eight to 20-plus nucleosomes, suggested by some as a higher-order chromatin structure. The superbead model proposes that the chromatin fiber consists of a string of those clusters. Electron microscopy under conditions that promote superbead formation shows that the size of the superbead is correlated with the length of the linker DNA. I would argue strongly that the superbeads are an artifact of decomposition of the structure, which occurs in solution or on the microscope grid. The size of the units thus formed seem to be related to the widths of the fibers in the intact state.

WIDOM: In collaboration with A. Klug, J. T. Finch, and J. O. Thomas in Cambridge, I have used electron microscopy and x-ray diffraction from oriented specimens to study the structure of the 300 Å chromatin filament *in vitro* (Widom and Klug, 1985. *Cell.* 43; Widom et al., 1985. *EMBO (Eur. Membr. Biol.)* 4; Widom, 1985. submitted for publication). The full set of bands (340, 110, 57, 37, and 27 Å) indicative of the 300-Å filament state and characteristic of chromatin *in vivo* (Langmore, J. P. and J. R. Paulson. 1983. *J. Cell Biol.* 96:1120–1131) is observed, and each band is found to have enhanced intensity in certain directions. The band at 110 Å is meridional; the bands at 340, 57, 37, and 27 Å are equatorial. The equatorially enhanced intensity extends inward from a peak at 57 Å toward 100 Å. The equatorial 340 Å band is due to interference between laterally packed 300 Å filaments, preferentially oriented parallel to the capillary axis. The meridional 110 Å band, and the equatorial 57–100 Å diffraction are due, respectively, to the edge-to-edge packing of nucleosomes in the direction of the 300-Å filament and the radial packing around it. The equatorial bands at 37 and 27 Å are due to diffraction internal to nucleosome core particles. This interpretation of the diffraction patterns has been confirmed by calculating diffraction patterns of models, based on the Cambridge nucleosome core particle structure. Additional calculations, in which the density of the solvent is varied in the computer, show that the 27-Å band is due to the organization of DNA on the core particle; the 37-Å band has contributions for both DNA and protein organization. The packing of nucleosome specified by these patterns is consistent with the solenoid model of Finch and Klug.

These diffraction patterns specify the packing of nucleosomes, but not their connectivity. Other models can be constructed which are consistent with these patterns, yet differ in their DNA linker paths from the solenoid, in that laterally neighboring nucleosomes come from nonconsecutive locations along the DNA.

These different models imply different effects of a changed linker length. We therefore carried out electron microscopy and x-ray diffraction experiments to study the higher-order structure of sea urchin sperm chromatin, which has the longest reported repeat length, −240 bp. By comparing the results from sea urchin sperm chromatin with those from chicken erythrocyte 300-Å filaments (repeat length −212 bp), we determine the effects on higher order structure due to the addition of 28 bp (−100 Å) of linker DNA.

Electron micrographs, taken in a wide range of conditions, show that sea urchin sperm chromatin forms filaments with a diameter of −300 Å, which are no wider than those of chicken erythrocyte chromatin under the same conditions. Additionally, partially oriented x-ray patterns from sea urchin sperm chromatin show the same spacings and orientations of the bands due to nucleosomal packing as were found for chicken erythrocyte chromatin. Therefore, we conclude that linker DNA is not contributing significantly as a structural component to the 300-Å filament, and must be bent and looped clear of the contacts between nucleosomes.

Resolution of the differences between our results and those of Williams et al. must await further work, bearing in mind that one must be certain that one is studying properties of monomeric filaments, and not aggregates which could have an increased diameter and mass per unit length.

KOCH: There are two papers coming out soon by J. Bordas, L. Perez-Grau, M. C. Vega, C. Nave, and myself, (J. L. Bordas et al., *Europ. Biophys. J.*, in press) which give the interpretation of an extensive small angle scattering study of chicken erythrocyte chromatin using synchrotron radiation. Then experiments were done on solutions and gels of chromatin fragments (70–90 nucleosomes) and on nuclei at different ionic strengths. In the model we propose, chromatin in solution at low ionic strength has a preformed helical structure held together by the H1 (H5) histones with a pitch of 30 nm, a diameter of ~ 30 μM, similar to that of condensed chromatin and about three nucleosomes per turn. After condensing, the structure folds like an accordian by reduction of the pitch to ~ 3 nm in <50 ms. In this model the main contribution to the 20 nm feature, which is a very specific marker of the degree of condensation, would come from a layer line with a near-meridonal peak intensity. This interpretation is supported by the fact that when the length of the linker is increased by binding of ethidium bromide or during thermal denaturation (M. C. Vega, Ph.D. thesis, 1985) the 20-nm feature shifts to lower angles, while the mass-per-unit length and the radius of gyration of the cross-section decrease. It should be stressed that under similar conditions of ionic strength the data obtained by the different groups are identical, but a different interpretation is placed on them. One of the causes of discrepancy is that in several instances (Suau et al. 1979. *Eur. J. Biochem.* 97:593; Hollandt et al. 1979. *Nucleic Acid Res.* 6:2017) the radii of gyration of the cross-section have been obtained by extrapolation of a region beyond the maximum of the 20 nm feature ($s > 0.05$ nm^{-1}). The only experimental data that differ from ours is that of Sperling and Tardieu (1976, *FEBS (Fed. Eur. Biochem. Soc.) Lett.* 64:89). They did not observe the 20-nm feature in their preparations of rat liver chromatin at low ionic strength, whereas we do see this with our rat liver chromatin preparations.

LANGMORE: The solenoid model is the simplest way to pack nucleosomes into a thick fiber, and thus it is the most attractive model in the absence of contradictory experimental data. Although the MRC group has shown that their poorly oriented diffraction patterns are consistent with the solenoid model, Dr. Widom has agreed that the patterns are also consistent with the crossed-linker model. I would add that these patterns are also consistent with a range of nonhelical models, because the indicative "helical-cross" pattern was not evidenced in the MRC data. Thus, I believe that Dr. Widom's conclusions about the helical parameters and the origins of each of the diffraction bands are premature.

More importantly, I find recent evidence to be inconsistent with the solenoid model. Specifically, (*a*), the absolute mass-per-unit length of the chromatin fibers has been measured by Woodcock et al. and by us to be considerably larger than six nucleosomes per 11 nm; (*b*), the diameter of the fibers has been measured to be larger than 30 nm; and (*c*), all

of the above measurements are correlated with the linker length. The solenoid model cannot account for any of these data.

Dr. Widom has suggested that the discrepancies between the MRC data and ours is due to aggregation of chromatin. There is no evidence of such aggregation in any of our microscopy nor that of Woodock et al. Furthermore, Dr. Widom's own studies of chromatin under different ionic conditions have not demonstrated aggregation under the conditions used for the microscopy.

I suggest that the Cambridge studies might have been unable to show a "20-nm" reflection because they used chicken erytrhrocyte chromatin, which is less ordered than other types of chromatin, and they used nonphysiological polyvalent ions to aggregate the chromatin into macroscopic fibers. Bordas et al. and we find that the "20-nm" reflection disappears under conditions where the fibers are packed side-by-side. We interpret this as simple lattice interference with the inherent fiber contrast at "20 nm." The failure of the Cambridge studies to detect a difference between the fiber diameters of chicken and sea urchin chromatin might have resulted from the use of a ruler (as Dr. Widom has stated in this discussion) rather than a densitometer to measure the micrographs. Since Widom et al. do not present histograms or standard deviations in their publications, we cannot say whether their measurements were accurate enough to detect the difference in fiber diameter.

I feel that the studies presented by Dr. Koch are consistent with our observations and crossed-linker model. They have observed a "10-nm" feature in partially unfolded chromatin, which seems to have a different origin than the sharper "20-nm" reflection that we observe at physiological salt. In agreement with Koch, we see evidence of higher order structure at low ionic strength, in disagreement with the data of Sperling and Tardieu. Although the model of Koch agrees with our x-ray data, it is not consistent with our measurements of mass per unit length or our interpretations of the Fourier transforms of the electron micrographs.

I think that the double-helical crossed-linker model is the simplest pattern of nucleosome assembly that fits the existing structural data. The model is highly constrained by steric conditions and thus can be critically tested by further x-ray, microscopic, and hydrodynamic experiments. Although we know that the fibers are not as straight and highly ordered as other filamentous structures such as microtubules and f-actin, we hope that further work will better define the basic pattern of nucleosome packing into thick fibers, and elucidate how perturbations in that pattern affect the folding and function of chromatin in living cells.

MAKOWSKI: These last few comments have been close to my heart in that they have been concerned with how to obtain the maximum amount of information from a minimum amount of data. The problem is profoundly difficult because we are applying techniques that are optimum for ordered structures to a system that has spatial disorder and, given linker length variations, chemical disorder as well. Present DNA technology allows me to hope for a way to produce chemically ordered structures by reassembling nucleosomes along chemically identical steps in hopes of obtaining a spatially ordered system more amenable to study.